

Accepted Manuscript

Multi-isotopic tracing (Mo, S, Pb, Re—Os) and genesis of the Mo—W Azegour skarn deposit (High-Atlas, Morocco)

Éric Marcoux, Noémie Breillat, Catherine Guerrot, Philippe Négrel, Samia Berrada Hmima, David Selby

PII: S1464-343X(19)30114-1

DOI: <https://doi.org/10.1016/j.jafrearsci.2019.04.007>

Reference: AES 3481

To appear in: *Journal of African Earth Sciences*

Received Date: 21 November 2018

Revised Date: 8 April 2019

Accepted Date: 8 April 2019

Please cite this article as: Marcoux, É., Breillat, Noé., Guerrot, C., Négrel, P., Hmima, S.B., Selby, D., Multi-isotopic tracing (Mo, S, Pb, Re—Os) and genesis of the Mo—W Azegour skarn deposit (High-Atlas, Morocco), *Journal of African Earth Sciences* (2019), doi: <https://doi.org/10.1016/j.jafrearsci.2019.04.007>.

This is a PDF file of an unedited manuscript that has been accepted for publication. As a service to our customers we are providing this early version of the manuscript. The manuscript will undergo copyediting, typesetting, and review of the resulting proof before it is published in its final form. Please note that during the production process errors may be discovered which could affect the content, and all legal disclaimers that apply to the journal pertain.



Multi-isotopic tracing (Mo, S, Pb, Re-Os) and genesis of the Mo-W Azegour skarn deposit (High-Atlas, Morocco)

2019, February 25th

Éric Marcoux (1), Noémie Breillat (2), Catherine Guerrot (3), Philippe Négrel (4),
Samia Berrada Hmima (5), David Selby (6)

(1) Corresponding author

University of Orléans, ISTO, UMR 7327, 45071, Orléans, France

eric.marcoux@univ-orleans.fr

(1), (2), (3) and (4) - BRGM, ISTO, UMR 7327, BP 36009, 45060 Orléans, France - CNRS/INSU, ISTO, UMR 7327, 45071 Orléans, France - University of Orléans, ISTO, UMR 7327, 45071, Orléans, France

(5) - Laboratoire Géo-Ressources, URAC 42, Département de Géologie, Faculté des Sciences et Techniques de Marrakech, Université Cadi Ayyad, Marrakech, Morocco

(6) - Department of Earth Sciences, Durham University, Durham DH1 3LE, UK - State Key Laboratory of Geological Processes and Mineral Resources, School of Earth Resources, China University of Geosciences, Wuhan, China

Regular Article submitted to Journal of African Earth Sciences –
Revised version

Abstract

The Mo-Cu-W Azegour skarn, located in the High-Atlas in Morocco, is associated with a Late Hercynian alkaline granitic intrusion. Here the origin of the mineralisation via Re-Os geochronology and using Mo, S and Pb isotopes is discussed. The age of mineralization defined by Re-Os molybdenite geochronology is 276 ± 1.2 Ma for the Azegour mine, and 267 ± 1.2 for the Tizgui deposit suggesting for multiple mineralization events associated with the Hercynian alkaline granitic intrusion. The $\delta^{98}\text{Mo}_{\text{NIST}}$ of molybdenite range from -0.60 ‰ to 0.42 ‰ ($n=26$) for the Azegour mine and from 0.08 ‰ to 0.40 ‰ ($n=2$) for the Tizgui mine. Variations of the $\delta^{98}\text{Mo}_{\text{NIST}}$ occur either at the deposit scale with a difference of about 0.72 ‰, and at the sample scale (few cm), which exhibits a difference of up to 0.40 ‰. A multi-phased mineralization is proposed as the main processes explaining the variation in the $\delta^{98}\text{Mo}_{\text{NIST}}$ values although the influence of a Rayleigh fractionation process cannot be precluded. The high $\delta^{34}\text{S}$ values determined from molybdenite, pyrrhotite, and chalcopyrite (8 to 14.7 ‰) suggest a sedimentary origin for sulphur from the Cambrian sedimentary country rocks. Whereas, the initial $^{206}\text{Pb}/^{204}\text{Pb}$ compositions of common lead (18.08 to 18.30) for

37 chalcopyrite and pyrrhotite imply a strong contribution of lead from the host volcano-sedimentary
38 units.

39

40 **Keywords:** Azegour skarn, molybdenite, molybdenum, lead, sulphur, isotopes, Re-Os geochronology,
41 mineralization

42

43 **1. Introduction**

44 Skarns are among the most common types of deposit in the world and have been
45 widely studied. They form large deposits of tungsten, lead-zinc, copper and gold, and also
46 yield tin in the form of cassiterite, and very seldomly, molybdenum.

47 The present study focuses on the Azegour Mo-skarn in Morocco. Located in the High-
48 Atlas, the Azegour site (Fig. 1) is a Mo-W-Cu skarn with production from three historic mines:
49 main Azegour, by far the main one, Tizgui and Entifa. This skarn was exploited from 1932 to
50 1959 supplying 1300 t of MoS₂. The Mo content is estimated around 8000 t (Permingeat,
51 1957). A re-opening of the mine is possible. Molybdenite is not the only economically
52 important mineral in the Azegour skarn, scheelite and chalcopyrite were reported at
53 economic grades (Permingeat, 1957). The existence of Mo mineralization and deposits in this
54 area occurs over more than 3.5 km (Fig. 2).

55 ***Figure 1: Location of the Azegour skarn in North part of Moroccan High-Atlas***

56 Molybdenum (Mo) isotopes are commonly used to investigate (paleo-)redox conditions, Mo
57 input into the oceans from weathering, and more recently, as with other transition-meta
58 isotopes, for studying trace-metal pollution (Archer and Vance, 2008). In the frame of
59 mineral resources, only few studies have been performed regarding Mo isotopes in
60 molybdenite. These studies have principally focused on molybdenite in pegmatite veins
61 (Greber et al., 2011), and porphyry systems (Greber et al., 2014; Shafiei et al., 2015) and on

62 other molybdenite-bearing ore deposits (Hannah et al., 2007; Mathur et al., 2010; Breillat et
63 al., 2016). These studies suggest that the influence of the crystallisation temperature, stage
64 of crystallisation, Rayleigh processes and crystal structure (2H or 3R polytypes) are factors
65 that control the Mo isotopic composition.

66 Here we utilize Mo, together with Pb and S isotope data of sulphides and gangue
67 minerals and Re-Os molybdenite geochronology to provide an improved understanding of
68 the genesis of the Mo mineralisation of the Azegour skarn deposit system.

69 **2. Geological context**

70 The molybdenum-copper Azegour skarn in Morocco is located 60 km south of Marrakech
71 in the northern boundary of High Atlas Mountains (Fig. 1) (coordinates: 31°09'16" N,
72 8°18'19" W). Numerous studies have discussed the geology of the Azegour skarn over the
73 past 80 years (e.g., Moret, 1931; Heim, 1934; Permingeat, 1957; El Amrani, 1984 and
74 Berrada et al., 2011, 2015). The skarn formed as the result of the intrusion of a Permian
75 granite into a series of volcano- sedimentary units (Fig. 2 and 3) dated Cambrian by the
76 presence of Archoeocyathides (Neltner, 1938).

77 ***Figure 2: Geological map of the Azegour region. Figure 2 is fully contained in the red***
78 ***triangle on figure 1***

79 The volcano-sedimentary series are composed of grey to black shales, a volcanic unit (with
80 dominant andesitic flows and dacitic pyroclastic rocks), marbles, recrystallized limestone and
81 dolostone. A Late Hercynian alkaline granitic intrusion (Lagarde, 1987; Mrini et al., 1992),
82 named the Azegour granite, outcrops for 7 km along a NW-SE direction with a 1 km width.
83 The skarn is developed within the Palaeozoic volcano-sedimentary units (Fig. 2).

84 **Figure 3: Granite and skarn contact in Azegour**

85 The Azegour granite is hyperaluminous (Lagarde, 1987; Ait Ayad et al., 2000) and is mainly
86 composed of quartz, feldspar (orthoclase and plagioclase), and minor biotite. The granite
87 crystallisation is dated at 269 ± 11 Ma (Charlot et al., 1967) and 271 ± 3 Ma (Mrini, 1985) by
88 the Rb-Sr method. The Sr and Nd initial ratios ($I_{Sr} = 0.7051$; $\epsilon_{Nd(T)} = -1$; $T = 270$ Ma) obtained
89 on the Azegour granite suggest a composite origin (crust-mantle) with a strong mantle
90 component (Mrini, 1985; Mrini et al., 1992). Metasomatized carbonate layers constituting
91 the skarn are several meters thick, and are mainly composed of massive garnetite and/or
92 wollastonite-rich rock, with rare pyroxenite. Garnets belong to three different types: a
93 green-black garnet is very common, forming crystals up to 8 cm, and composed of andradite
94 with locally a core of Al-rich andradite (up to 5 % Al_2O_3); a very common brown-black garnet
95 forms thick layers associated with quartz and commonly reveals a core of pure andradite
96 surrounded by a Al-rich andradite (up to 10 % Al_2O_3), close to a grossular type, and an
97 orange garnet (Toulkine village zone) that is composed of only grossular garnet. The
98 abundance of spessartine is always low (4 % maximum). Wollastonite is slightly
99 manganese-rich, whereas vesuvianite is F- and Cl-rich (up to 3.3 % and 1.2 %, respectively).

100 The mineralogical assemblage suggests the formation of the prograde stage of the skarn
101 occurred at around 620 - 650 °C, under a pressure of 1.7 - 2 kbar, and a fCO_2 of 31 mole %, in
102 a reducing environment (fO_2 of 10^{-18} to 10^{-16} atm.), preceding a retrograde stage. Sulphides
103 formed during the retrograde stage (< 450 °C) (Berrada et al., 2015). The garnetites are the
104 main Mo-bearing rocks in the form of large (up to 3 cm) molybdenite crystals (Fig. 4). Similar
105 to molybdenite, scheelite occurs only in garnetite, whereas chalcopyrite and pyrrhotite (Fig.
106 5) are mainly associated with pyroxenite. The skarn is widely overlain by Cretaceous
107 formations.

108 **Figure 4: Coarse molybdenite (white and grey) within garnetite from the Azegour mine.**
109 **Photograph in reflected light**

110 **Figure 5: Chalcopyrite (C, yellow) and pyrrhotite (Po, light brown) from Azegour mine.**
111 **Photograph in reflected light**

112 3. Methodology

113 3.1. Molybdenum isotopic composition

114 The analyses of molybdenum isotopic composition have been performed at BRGM (France)
115 on 29 samples of molybdenite. The procedure for analysing the Mo isotopic composition in
116 molybdenite has been described in detail in Breillat et al. (2016). As Mo is the major cation in
117 molybdenite (59.94 %), no chemical purification prior to analysis was undertaken (Anbar et
118 al., 2001; Barling et al., 2001; Malinovsky et al., 2007; Mathur et al., 2010). Mathur et al.
119 (2010) evaluated possible matrix effects induced by the lack of chemical purification for
120 molybdenite by analysing the same sample with or without purification and both results
121 were in agreement. Around 100 mg of molybdenite (single grain for large crystals, multiple
122 grains for disseminated molybdenite) was handpicked and then finely crushed in order to
123 homogenize the sample. Around 10 mg of molybdenite powder were dissolved in 4 ml of
124 *aqua regia* (1 ml of HNO₃ 7N and 3 ml of HCl 8N) at 100 °C in PTFE beakers until complete
125 dissolution. The solutions were dried and the residues were dissolved in 10 ml of HNO₃ 3 %
126 (v/v). From this concentrated solution, a final solution was prepared in HNO₃ 3 % in order to
127 get a final Mo concentration of 1 µg.ml⁻¹ (allowing a signal of around 2.5 V on mass ⁹⁵Mo).
128 Zirconium was added to this solution to yield a concentration of 0.5 µg.ml⁻¹ (allowing a signal
129 of around 4 V on mass ⁹⁰Zr). The Mo blank level for the whole procedure is less than 0.05 %
130 and thus negligible as compared to the sample concentration.

131 The Mo-isotopic composition analyses were performed using an MC-ICP-MS Neptune
132 (Thermo-Finnigan). Zirconium (Zr) and ruthenium (Ru) produce several isobaric interferences
133 on 92, 94, 96 and 96, 98, 100 masses, and only ^{95}Mo and ^{97}Mo are free of interference. Such
134 interference is easily corrected with the following cup configuration: $^{90}\text{Zr-L3}$, $^{91}\text{Zr-L2}$, $^{92}\text{Mo-}$
135 $^{92}\text{Zr-L1}$, $^{94}\text{Mo-}^{94}\text{Zr-Ax}$, $^{95}\text{Mo-H1}$, $^{97}\text{Mo-H2}$, $^{98}\text{Mo-}^{98}\text{Ru-H3}$, $^{99}\text{Ru-H4}$. In our samples and
136 standards, ruthenium has never been detected. The Mo-isotope measurements were run
137 within sequences composed of blank, standard and sample analyses. After the sample and
138 standard analyses, two minute washes (HNO_3 3 %) are done to get the low background
139 values (less than 5 mV). The reported data represent the mean value of a minimum of 5 runs
140 of 20 measurements. Mass bias was corrected by $^{90}\text{Zr}/^{91}\text{Zr}$ external spiking (Zirconium ICP
141 standard CertiPUR Merck) at $0.5 \mu\text{g}\cdot\text{ml}^{-1}$ (Anbar et al., 2001) and standard-sample-standard
142 bracketing. The external long-term reproducibility obtained during the course of this study
143 was 0.08 ‰ (2σ , $n = 137$) for an ICP standard solution (Techlab n°B3015042). In order to test
144 the reproducibility of our procedure on the same matrix, a Re-Os molybdenite standard
145 (Henderson Molybdenite Reference Material 8599 [RM8599], Markey et al., 2007) has been
146 repeatedly analysed as a secondary standard. All data are reported as classic $\delta^{98}\text{Mo}_{\text{NIST}}$ units
147 relative to a standard solution, in this case NIST SRM 3134 (lot # 891307), according to the
148 following formula (Eq. 1):

$$149 \quad \delta^{98}\text{Mo}_{\text{NIST}} = \left[\frac{(^{98}\text{Mo}/^{95}\text{Mo})_{\text{sample}}}{(^{98}\text{Mo}/^{95}\text{Mo})_{\text{standard}}} - 1 \right] * 1000 \quad (\text{Eq. 1})$$

150 The NIST SRM 3134 solution (lot#891307) has been proposed as a reference for reporting
151 Mo-isotopic compositions (Wen et al., 2010; Greber et al., 2012; Goldberg et al., 2013).
152 Following Goldberg et al. (2013), the $\delta^{98}\text{Mo}_{\text{NIST}}$ of NIST SRM 3134 is defined as 0 ‰ and data
153 are reported according to this value. The reference material 8599 yielded a $\delta^{98}\text{Mo}_{\text{NIST}}$ of -

154 $0.20 \pm 0.08 \text{ ‰}$ (2σ , $n = 85$; Breillat et al., 2016). Variation between samples is expressed as
155 $\Delta^{98}\text{Mo}$ which corresponds to the difference between the maximum and the minimum values
156 of $\delta^{98}\text{Mo}_{\text{NIST}}$.

157 **3.2. Sulphur isotopic composition**

158 The sulphur isotopic compositions were measured in BRGM (France) for molybdenite,
159 chalcopyrite and pyrrhotite samples from the Azegour skarn. Molybdenite flakes were
160 handpicked, and then crushed in agate bowl. Chalcopyrite and pyrrhotite were collected
161 using a Dremel™ drill. Around 100 to 150 μg of the obtained powder with pentoxide of
162 vanadium as catalyser were placed into a tin capsule. Analyses were performed on
163 Elementary Analyser IRMS Delta V Plus (Thermo Finnigan). Sulphides were converted to SO_2
164 with a flash combustion at 1 000 °C and analysed after chromatographic separation. At least
165 two replicates were performed. All data are reported as classic $\delta^{34}\text{S}_{\text{VCDT}}$ units relative to vCDT
166 standard according to the following formula (Eq. 2):

$$167 \quad \delta^{34}\text{S}_{\text{VCDT}} = \left[\frac{(^{34}\text{S}/^{32}\text{S})_{\text{sample}}}{(^{34}\text{S}/^{32}\text{S})_{\text{standard}}} - 1 \right] * 1000 \quad (\text{Eq. 2})$$

168 **3.3. Lead isotopic composition**

169 Lead isotopic compositions of molybdenite, chalcopyrite, pyrrhotite samples from the
170 Azegour skarn and K-feldspar from the Azegour granite have been measured in BRGM
171 (France) according to techniques adapted from Marcoux (1987) and Pomiès et al. (1998).
172 After cleaning, sulphides (50 to 100 mg) are dissolved with a mixture of HNO_3 7N – HCl 6N
173 and a drop of concentrated HBr in a Teflon container. Feldspars (200 mg) were dissolved in a
174 closed container by using a $\text{HF-HNO}_3\text{-HClO}_4$ mixture at 120 °C for one week. After
175 evaporation, the residue was dissolved by using HCl 6N, and heat again at 120 °C for one

176 week. After complete dissolution (sulphides and feldspars), the solutions were dried and
177 then dissolved with 3-4 ml of HBr 1N. The Pb was separated on quartz columns filled with 1
178 ml AG1X8 ion exchange resin by using HBr and HCl acids. The lead fraction is then purified on
179 a small 0.1 ml column by using HCl. After evaporation the residue was then recollected with
180 HNO₃ and dried again. Blanks for the overall procedure are lower than 100 pg and are
181 negligible relative to the amount of sample analyzed. Measurements of the lead ratios
182 (²⁰⁶Pb/²⁰⁴Pb, ²⁰⁷Pb/²⁰⁴Pb and ²⁰⁸Pb/²⁰⁴Pb) were obtained on static mode on a multicollector
183 MAT262 Thermal Ionisation Mass Spectrometer. Samples and standards were loaded on a
184 zone-refined Re filament previously outgassed. Silica gel was used as an emission stabilizer.
185 About 150 ng of lead were loaded with H₃PO₄ onto each filament. The Pb isotopic ratios
186 were corrected for a mass bias of 0.14 % per amu (atomic mass unit) determined by
187 repeated measurements of the NBS982 standard. Individual error on all ratios is commonly
188 better than 0.01% (2σ_m), whereas external reproducibility (2σ) is 0.06 % for the ²⁰⁶Pb/²⁰⁴Pb,
189 0.09 % for the ²⁰⁷Pb/²⁰⁴Pb and 0.12 % for the ²⁰⁸Pb/²⁰⁴Pb.

190 For chalcopyrite, pyrrhotite, molybdenite and K-feldspar, Pb, U and Th contents of the
191 sample were used for correcting the measured Pb isotope ratios for the addition of
192 radiogenic Pb, assuming a mean age of 270 ± 10 Ma. These corrections are insignificant for
193 most of the samples due to very low U/Pb and Th/Pb values, except for AZT1a pyrrhotite
194 (²³⁸U/²⁰⁴Pb = 15.7). However, the corrected ratios for this sample are in the range of the
195 other sulphides. For molybdenite (Mo4, Mo7, Mo8; ²³⁸U/²⁰⁴Pb = 0.1, 5.9 and 11.4
196 respectively) corrected values remain more radiogenic than the other sulphides.

197 **3.4. Re-Os isotopic composition**

198 The Re-Os analyses were performed on 3 samples of molybdenites. Samples were prepared
199 in BRGM (Orléans, France), with the chemical and mass spectrometry protocols performed
200 at Durham University (UK) in the Laboratory for sulphide and source rock geochronology and
201 geochemistry and the Arthur Holmes Laboratory, members of the Durham Geochemistry
202 Centre. Molybdenite separates of the 125 – 250 μm fraction were obtained by traditional
203 methods (crushing, heavy liquids, magnetic separator and handpicking under a microscope
204 to remove impurities).

205 The procedure for the Re-Os analyses is described in detail in Selby and Creaser (2001a, b).
206 The Carius tube method (Shirey and Walker, 1995) was used for dissolution of the
207 molybdenite and equilibration with the tracer solution (^{185}Re + normal Os). Osmium was
208 separated and purified by CHCl_3 solvent extraction and micro-distillation. The rhenium was
209 separated and purified using NaOH-acetone solvent extraction and anion chromatography.
210 The purified Re and Os fractions were loaded onto Ni and Pt wire filaments, respectively, and
211 analysed for their isotope composition by negative thermal ionisation mass spectrometry
212 (NTIMS) of a Triton Scientific mass spectrometer. Molybdenites have naturally high Re
213 content and no initial Os (Morgan et al., 1968; Markey et al., 1998), all the ^{187}Os is derived
214 from the decay of ^{187}Re (Faure, 1986). Model Re-Os ages were calculated using the equation
215 $\ln(^{187}\text{Os}/^{187}\text{Re} + 1)/\lambda$, using the decay constant (λ) of $1.666\text{e}^{-11}\text{a}^{-1}$ (Smoliar et al., 1996).
216 Uncertainties include all sources of analytical uncertainty (Re and Os mass spectrometer
217 measurements, blank abundances and isotopic compositions (Re = 3.2 ppt; Os = 0.3 ppt;
218 $^{187}\text{Os}/^{188}\text{Os} = 0.223 \pm 0.03$, n=1), spike calibrations and reproducibility of standard Re and Os
219 isotopic values), and with and without the uncertainty in the decay constant (0.35 %; Smoliar
220 et al., 1996; Selby et al., 2007).

221 4. Results

222 4.1. Re-Os

223 The results of Re-Os analyses on molybdenites are given in Table 1. The Re and ^{187}Os
224 concentration for Tizgui MoS_2 are respectively 14.00 ± 0.05 ppm and 39.35 ± 0.13 ppb. The
225 Re concentration for the two Azegour MoS_2 is 7.00 ± 0.03 ppm and 2.87 ± 0.01 ppb and the
226 ^{187}Os concentration is 20.31 ± 0.07 ppb and 8.33 ± 0.02 ppb.

227

228 ***Table 1: Re-Os data and model dates for molybdenites analyzed in this study.***

229 The Re-Os model age for the Tizgui mine sample is 267.79 ± 1.45 Ma, whereas the Re-Os
230 ages for the Azegour mine are almost 10 Ma older (276.56 ± 1.51 Ma and 276.84 ± 1.49 Ma;
231 Table 1).

232 4.2. Molybdenum

233 The molybdenite from Azegour skarn display $\delta^{98}\text{Mo}_{\text{NIST}}$ values that range between -0.60 ‰
234 and $+0.42$ ‰ (Fig. 6 and Table 2) resulting in a variation of $\Delta^{98}\text{Mo} = 1.02$ ‰. Such a variation
235 at the scale of a deposit is coherent with the variations for other occurrences or deposits
236 shown by previous studies. For example, Mathur et al. (2010) found a $\Delta^{98}\text{Mo}$ of around 0.75
237 ‰ for El Teniente ore deposit in Chile. A slightly larger variation was shown by Greber et al.
238 (2011) for the Grimsel Pass pegmatite ($\Delta^{98}\text{Mo}$ of ~ 1.14 ‰) and for the Alpjahorn pegmatite
239 $\Delta^{98}\text{Mo}$ of ~ 1.35 ‰). Greber et al. (2014) found a $\Delta^{98}\text{Mo} = 0.88$ ‰ in the Questa porphyry Mo
240 ore deposit (New Mexico, USA). Additionally, Shafiei et al. (2015) reported the largest
241 variation ($\Delta^{98}\text{Mo}$ of around 1.94 ‰) for the Kerman porphyry deposit (Iran).

242 **Figure 6: Histogram of Mo isotopic composition of molybdenite samples from Azegour**
243 **mine and Tizgui mine**

244 The mean $\delta^{98}\text{Mo}_{\text{NIST}}$ value for the molybdenite samples of the Azegour skarn is -
245 $0.01 \pm 0.56 \text{ ‰}$ (2σ , $n=29$). This value fully agrees with the mean value of molybdenites
246 analysed in all literature and normalized to NIST 3134 as summarized by Breillat et al. (2016)
247 ($0.04 \text{ ‰} \pm 1.04 \text{ ‰}$, 2σ , $n=391$).

248 We investigated the possible variation of the $\delta^{98}\text{Mo}_{\text{NIST}}$ of the Azegour skarn by
249 analysing two samples collected in the Tizgui mine, located 2 km to the North of the Azegour
250 mine. The molybdenite crystals of the two sites show distinct differences: massive and
251 centimetre in size (up to 5 cm) in the Azegour mine, disseminated and millimetre in size
252 (maximum 7 mm) in the Tizgui mine. The $\delta^{98}\text{Mo}_{\text{NIST}}$ values are 0.08 ‰ and 0.40 ‰ in the
253 samples from the Tizgui mine, whereas the values for the Azegour mine are between -0.60
254 ‰ and $+0.42 \text{ ‰}$ (Table 2). The variation within individual samples from $-0.17 \pm 0.11 \text{ ‰}$ to
255 $0.42 \pm 0.13 \text{ ‰}$ (Mo076, Table 2), giving a $\Delta^{98}\text{Mo}$ of around 0.59 ‰ , is similar to the whole
256 variation measured in the Tizgui mine and not significantly different to variations measured
257 in this study.

258 Greber et al. (2011) and Shafiei et al. (2015) found evidence of multi-modality in the
259 distribution of the $\delta^{98}\text{Mo}_{\text{NIST}}$ in molybdenites. On the contrary, in the Azegour skarn, the
260 distribution of the data follows a Gaussian (normal) distribution, but nonetheless there is no
261 clear evidence of multi-modality in the distribution of the $\delta^{98}\text{Mo}_{\text{NIST}}$ in the molybdenites as
262 illustrated in the Figure 6. Given that the multi-modality is typically interpreted as
263 representing different phases of crystallisation, the Gaussian (normal) distribution may

264 suggest that only one phase of crystallisation has occurred, what is clearly not the case in the
265 Azegour skarn.

266 **Table 2: Mo-isotope data of molybdenites analyzed for this study. Data are relative to**
267 **NIST3134 ($\delta^{98}\text{Mo}_{\text{NIST}}=0$). N = number of analyses for each sample. Long-term external**
268 **reproducibility of 0.08 ‰ (2 σ) on $\delta^{98}\text{Mo}_{\text{NIST}}$. References to sub samples are indicated by an**
269 **additional subscript a to d, meaning up to 4 subsamples, i.e. same rock sample referred**
270 **MoXXX and up to 4 samples of molybdenite grain in the samples MoXXX.**

271 4.3. Sulphur

272 The molybdenites from the Azegour skarn have $\delta^{34}\text{S}_{\text{VCDT}}$ values ranging between 12.4 and
273 14.7 ‰ and the molybdenite samples collected in the Tizgui mine exhibit nominally lower
274 values (12.4 ‰, n=2) than those of the Azegour mine (12.7-14.7 ‰, n=27) (Table 3 and Fig.
275 7).

276 The $\delta^{34}\text{S}_{\text{VCDT}}$ values of chalcopyrite range between 10.5 and 12.5 ‰ (n=5). The $\delta^{34}\text{S}_{\text{VCDT}}$ for
277 the pyrrhotites from Tizgui mine are 8.0 and 8.3 ‰ (n=2), with the pyrrhotites from Azegour
278 mine possessing values of 12.2 and 14.2 ‰.

279 **Figure 7: Histogram of $\delta^{34}\text{S}_{\text{VCDT}}$ isotopic composition of molybdenite, chalcopyrite and**
280 **pyrrhotite samples**

281

282 **Table 3: Sulphur isotope data of molybdenites, chalcopyrites and pyrrhotites analyzed in**
283 **this study.**

284

285 4.4. Lead

286 Initial lead isotopic compositions ($^{206}\text{Pb}/^{204}\text{Pb}$, $^{207}\text{Pb}/^{204}\text{Pb}$ and $^{208}\text{Pb}/^{204}\text{Pb}$) calculated using a
287 mean age of 270 ± 10 Ma are reported in Table 4 and Figure 8. The range of the initial lead
288 isotope composition can be illustrated by the $^{206}\text{Pb}/^{204}\text{Pb}_i$ value, ranging for chalcopyrite,
289 pyrrhotite and feldspar samples from 18.08 to 18.30. Chalcopyrite $^{206}\text{Pb}/^{204}\text{Pb}_i$ values are
290 close (18.13 to 18.23), whereas pyrrhotite $^{206}\text{Pb}/^{204}\text{Pb}_i$ values exhibit a wider range from
291 18.08 to 18.30. The $^{206}\text{Pb}/^{204}\text{Pb}_i$ values for molybdenite are more radiogenic, between 18.51
292 and 20.01.

293 **Figure 8: Pb-Pb diagrams of initial composition of chalcopyrite, pyrrhotite, and K-feldspar**
294 **from Azegour granite (Mrini, 1985), with the Stacey-Kramers (1975) growth curve (SK) and**
295 **Doe-Zartman (1979) orogen curve. The measured ratios have been corrected for the**
296 **addition of radiogenic Pb, assuming an age of 270 Ma. Molybdenite corrected ratios are**
297 **too radiogenic and do not appear on this figure. Lead isotopic composition of neighbouring**
298 **ore deposits are mentioned for comparison: galena from Amensif ore deposit (Ilmen et al.,**
299 **2014) and from Draa Sfar and Hajar huge VMS (Marcoux et al., 2008).**

300 **Table 4: Lead isotope data of molybdenite, chalcopyrite, pyrrhotite and K-feldspar**
301 **analyzed in this study. Measured values have been corrected to an age of 270 Ma.**

302 5. Discussion

303 5.1. Re-Os dating of the molybdenites

304 The results are consistent with the age of the granite crystallisation dated at 269 ± 11 Ma
305 (Rb-Sr, Charlot et al., 1967) and 271 ± 3 Ma (Rb-Sr, Mrini, 1985). Therefore, we conclude that
306 the Mo mineralisation is contemporaneous with crystallisation of the Azegour granite.
307 However, a difference of a few million years can be observed between the molybdenite
308 sample from Tizgui (youngest) and samples from Azegour (oldest). Molybdenite records the
309 timing of mineralisation and by inference the age of the associated granite suggesting in this

310 case a multi-phased granitic intrusion. Such a magmatic-hydrothermal multi-phased history
311 is very common in porphyry and related-skarn ore deposits (Sillitoe, 2010) as well as in major
312 skarn deposits like Los Santos, Spain (Timon-Sanchez et al., 2009) and Salau, France
313 (Poitrenaud et al., in press) where two successive intrusions emplaced at 269 ± 6 and 280 ± 6
314 Ma (K/Ar dates), and 289.1 ± 1.9 Ma and 295 ± 2 Ma (LA-ICP-MS-U-Pb dates) respectively. At
315 Azegour we assume that the intrusion could also be multiple phased but of similar lithology
316 or, more likely, the presence of a younger intrusion at depth that gave way to the Tizgui
317 mineralization.

318 **5.2. Possible causes of Molybdenum isotopic composition variations**

319 Four processes are described in the literature to explain these variations at deposit scale and
320 even at sample scale. First, Klemm et al. (2008) suggested that the fractionation of the Mo
321 isotopes is due to the different stages of mineralisation, a progressive enrichment in heavy
322 Mo isotopes in the residual melt of subvolcanic magma chamber being the cause of the
323 variation in the Mo isotopes. The second process was described by Greber et al. (2014),
324 which argued for a fractionation of the Mo isotopes at the magmatic-hydrothermal
325 transition. A third process was first described by Hannah et al. (2007) and later by Klemm et
326 al. (2008), who suggested that fractionation that occurs during the same stage of
327 mineralisation, but also within an individual hand specimen, is due to a Rayleigh
328 fractionation of a hydrothermal fluid and a fractionation due to fluid phase separation (brine
329 and vapour). We recall that Rayleigh fractionation describes the evolution of a multi-phased
330 system, an hydrothermal system in this study, in which one phase is continuously removed
331 from the system through fractional distillation. This fractional distillation is one of the most
332 common cause of isotopic fractionation. Finally the last process was evoked by Shafiei et al.

333 (2015). They suggested that the fractionation of the Mo isotopes could be controlled by the
334 molybdenite structures (2H or 3R polytypes). When considering the whole variation of the
335 Mo isotopes observed in our data set, the variation within individual hand samples, the lack
336 of evidence of different values between the two sampling sites in Azegour and the two
337 different facies, we argue that the principal process of Mo fractionation in the Azegour skarn
338 is the succession of two phases of crystallisation evidenced by Re-Os molybdenite ages,
339 without precluding a probable influence of Rayleigh fractionation in the hydrothermal fluid.

340 **5.3. Source of ore-forming fluids: Sulphur isotopic composition**

341 The high values observed mostly within molybdenite for the Azegour skarn require a
342 contribution from a ^{34}S -enriched sulphur source. Magmatic sulphides in uncontaminated
343 felsic magmas generally have a signature value of $0 \pm 3 \text{‰}$ (Ohmoto, 1972; Hoef, 1997), in
344 agreement with Liu et al. (2014) that suggested that $\delta^{34}\text{S}$ of between 2 and 4 ‰ indicate a
345 magmatic sulphur source. Values for Cu-porphyry deposits are mostly between -5 ‰ and +5
346 ‰, with carbonate-hosted Pb-Zn ore deposits values from -20 ‰ and +20 ‰. Most skarns
347 have $\delta^{34}\text{S}$ values between -5 ‰ and +5 ‰ (e.g. Ault and Williams-Jones, 2004) indicating a
348 magmatic source for sulphur.

349 The high $\delta^{34}\text{S}$ values measured in Azegour fall outside the field values indicating a
350 predominantly magmatic origin of sulphur in skarn deposits. The Azegour skarn is not the
351 only skarn with high values of $\delta^{34}\text{S}$. Ishihara et al. (2000; 2002) observed a range from 11.1
352 ‰ to 14.8 ‰ for Geumseong molybdenum skarn deposits (Korea) and suggest that
353 extraction and migration of sulphur of the host carbonates into the skarn mineralization.
354 Rose et al. (1985) reported values from 6.3 to 19.9 ‰ for the Cornwall skarn (Pennsylvania,
355 USA). These high values of $\delta^{34}\text{S}$ are well explained by a sedimentary source of sulphur and, in

356 some cases, a marine sedimentary source or evaporites with high $\delta^{34}\text{S}$ of sulphur cannot be
357 precluded (e.g., Faure and Brathwaite, 2006). The Azegour skarn occurs in carbonate series
358 with black shales from the lower Cambrian (Neltner, 1938), which usually possess a $\delta^{34}\text{S} > 20$
359 ‰ (Jébrak and Marcoux, 2015), and are thus likely the dominant source of sulphur for the
360 skarn, but, given to the $\delta^{34}\text{S}$ values, a complementary source of sulphur, probably magmatic,
361 is also required.

362 **5.4. Source of ore-forming fluids: Lead isotopic composition**

363 These high values indicate the influence of a more radiogenic component in their genesis.
364 Uranium is very scarce and disseminated as tiny uraninite crystals, but Permingeat (1957)
365 noted that, at the mine scale, uranium is preferentially associated with molybdenite but
366 none uraninite inclusion has been observed in molybdenite. However, as initial lead isotopic
367 compositions calculated for molybdenite are still more radiogenic than for other sulphides,
368 explanations could be that Pb from molybdenite is sourced in the more radiogenic host
369 rocks, while Pb from other sulphides is sourced in the magmatic intrusion, what is supported
370 by sulphur isotopic results.

371 Ilmen et al. (2014) have performed Pb isotopic analyses on a galena from the Amensif
372 deposit, which is located 5 km in the south of Azegour skarn and is spatially associated with
373 the Azegour granite. The $^{206}\text{Pb}/^{204}\text{Pb}$ isotopic values of galena (18.05, Fig. 8), close to initial
374 isotopic values measured on Azegour sulphides, suggest that the Pb was sourced from the
375 Lower Paleozoic volcano-sedimentary units (Ilmen et al., 2014).

376 Our data (molybdenite not included) define a narrower range with a mean
377 $^{206}\text{Pb}/^{204}\text{Pb}$ value at 18.18 ± 0.07 (σ). The initial $^{206}\text{Pb}/^{204}\text{Pb}$ value of the skarn is around 18.08
378 - 18.30. Feldspar sample from the Azegour granite having a $^{206}\text{Pb}/^{204}\text{Pb}$ value of 18.20,

379 suggests that the granite cannot be considered as a major source for lead in the skarn,
380 although its role as an accessory source cannot be discarded.

381 **6. Summary of the origin of the ore-forming elements in Azegour**

382 The Re-Os analyses of molybdenite (~267 and 276 Ma) provide a robust geochronology for
383 the mineralisation of the Azegour skarn, which are broadly contemporaneous with the
384 previous emplacement history of the granite (Rb-Sr ages determined on the granite ranging
385 from 269 ± 11 to 271 ± 3 Ma). Although presently there is no evidence of multi-staged
386 emplacement of the Azegour granite, the Re-Os molybdenite dates do imply two phases of
387 mineralisation within the Azegour system, and thus the presence of a hidden younger
388 intrusion at depth. Multi-phased crystallisation is proposed as the principal process of Mo
389 fractionation in the Azegour skarn and could explain Mo isotopic variation in occurrence and
390 sample scale, whereas a Rayleigh fractionation in hydrothermal fluid cannot be precluded.
391 The ^{34}S -enrichment of the sulphide ores of the Azegour skarn suggests a strong participation
392 of surrounding rocks. Regarding lead isotopes, the location of all Azegour samples below the
393 Stacey and Kramers (1975) and just below Doe and Zartman (1979) orogen curves suggest
394 that the ore forming materials are derived from a mixture of upper crustal material with an
395 important contribution of mantle lead, a result in accordance with the previous Sr and Nd
396 isotopic studies (Mrini, 1985).

397 **Acknowledgments**

398 This work is part of Noémie Breillat PhD research supported by the Region Centre and the
399 Carnot-BRGM Institute. We thank Anne-Marie Desaulty, Anne-Marie Gallas, Anne-Thérèse
400 Montech, Alexandre Vrain, Antonia Hoffman, Chris Ottley and Geoff Nowell for their support
401 during laboratory work Rebecca Neely is thanked for her constructive remarks.

402 **References**

- 403 Ait Ayad, N., Ribeiro, M.L., Sola, A.R., Moreira, M.E., Dias, R., Bouabdelli, M., Ezzouhaira, H.,
404 Charif, A., 2000. Le Granite d'Azegour (Maroc) : cartographie géochimique et
405 interprétation géodynamique. *Comunicações do Instituto Geológico e Mineiro* 87,
406 155-164.
- 407 Anbar, A.D., Knab, K.A., Barling, J., 2001. Precise determination of mass-dependent
408 variations in the isotopic composition of molybdenum using MC-ICP-MS. *Analytical*
409 *Chemistry* 73, 1425-1431, DOI: 10.1021/ac000829w.
- 410 Archer, C., Vance, D. 2008. The isotopic signature of the global riverine molybdenum flux and
411 anoxia in the ancient oceans. *Nature geoscience*, Vol 1, 597-600.
- 412 Ault, K.M., Williams-Jones, A.E., 2004. Sulfur and lead isotope study of the EL Mochito Zn-Pb-
413 Ag deposit. *Economic Geology*, 99, 1223-1231.
- 414 Barling, J., Arnold, G.L., Anbar, A.D., 2001. Natural mass-dependent variations in the isotopic
415 composition of molybdenum. *Earth and Planetary Science Letters* 193, 447-457.
- 416 Berrada, S.H., Hajjaji, M., Belkabir, A., 2011. Mineralogical and geochemical features of the
417 wollastonite deposit of Azegour, Haut-Atlas (Morocco). *Journal of African Earth*
418 *Sciences* 60, 247-252, DOI: 10.1016/j.jafrearsci.2011.03.008.
- 419 Berrada Hmima, S., Marcoux, É., Hafid, A., 2015. Le skarn Mo-W-Cu à grenat, wollastonite,
420 pyroxène et vésuvianite d'Azegour (Haut-Atlas, Maroc). *Bulletin de la Société*
421 *Géologique France*, 186 (1), 21-34, DOI: 10.2113/gssgfbull.186.1.21.

- 422 Breillat, N., Guerrot, C., Marcoux, É., Négrel, Ph., 2016. A new global database of $\delta^{98}\text{Mo}$ in
423 molybdenites: A literature review and new data. *Journal of Geochemical Exploration*,
424 161 : 1-15. DOI: 10.1016/j.gexplo.2015.07.019,
- 425 Charlot, R., Tisserant, D., Vidal, P., Vidal, F., 1967. Rapport technique et quelques résultats.
426 *Compte Rendu d'Activité, Service Géologique, Maroc*, 126-137.
- 427 Doe, B.R., Zartman, R.E., 1979. Plumbotectonics, the Phanerozoic. *Geochemistry of*
428 *hydrothermal ore deposits*, 22-70.
- 429 El Amrani, E.H.I., 1984. Contribution à l'étude pétrologique, minéralogique, métallogénique
430 et de pétrologie structurale des formations de la région d'Azegour (Haut-Atlas
431 occidental, Maroc). Thèse Doctorat 3ème cycle. Faculté des Sciences, Nancy I. France.
- 432 Faure, K., Brathwaite, R.L., 2006. Mineralogical and stable isotope studies of gold-arsenic
433 mineralisation in the Sams Creek peralkaline porphyritic granite, South Island, New
434 Zealand. *Mineralium Deposita*, 40, 802-827.
- 435 Faure, G., 1986. *Principles of isotope geology*. New York, John Wiley and Sons, 589p.
- 436 Goldberg, T., Gordon, G., Izon, G., Archer, C., Pearce, C.R., McManus, J., Anbar, A.D.,
437 Rehkämper, M., 2013. Resolution of inter-laboratory discrepancies in Mo isotope
438 data: an intercalibration. *Journal of Analytical Atomic Spectrometry* 28, 724-735, DOI:
439 10.1039/C3JA30375F.
- 440 Greber, N.D., Hofmann, B.A., Voegelin, A.R., Villa, I.M., Nägler, T.F., 2011. Mo isotope
441 composition in Mo-rich high- and low-T hydrothermal systems from the Swiss Alps.
442 *Geochimica et Cosmochimica Acta* 75, 6600-6609, DOI: 10.1016/j.gca.2011.08.034.

- 443 Greber, N.D., Pettke, T., Nägler T.F., 2014. Magmatic–hydrothermal molybdenum isotope
444 fractionation and its relevance to the igneous crustal signature. *Lithos* 190-191, 104-
445 110, DOI: 10.1016/j.lithos.2013.11.006.
- 446 Greber, N.D., Siebert, C., Nägler, T.F., Pettke, T., 2012. $\delta^{98/95}\text{Mo}$ values and molybdenum
447 concentration data for NIST SRM 610, 612 and 3134: Towards a common protocol for
448 reporting Mo data. *Geostandards and Geoanalytical Research* 36-3, 291-300, DOI:
449 10.1111/j.1751-908X.2012.00160.x.
- 450 Hannah, J.L., Stein, H.J., Wieser, M.E., de Laeter, J.R., Varner, M.D., 2007. Molybdenum
451 isotope variations in molybdenite: Vapor transport and Rayleigh fractionation of Mo.
452 *Geology* 35, 703-706, DOI: 10.1130/G23538A.1.
- 453 Heim, A., 1934. The molybdenum mine at Azegour, Morocco, Society of Economic
454 Geologists, Inc. 29, 76-83.
- 455 Hoefs, J., 1997. *Stable Isotope Geochemistry*. 4th edition. Springer-Verlag, Berlin, 1-201.
- 456 Ilmen, S., Alansari, A., Bajddi, A., Ennaciri, A., Maacha, L., 2014. Mineralogical and
457 geochemical characteristics of the Amensif Cu, Pb, Zn, (Ag, Au) ore deposit, Western
458 High Atlas, Morocco. *Journal of Tethys* 2, 118-136.
- 459 Ishihara, S., Jin, M.S., Sasaki, A., 2000. Source diversity of ore sulfur from Mesozoic- Cenozoic
460 mineral deposits in the Korean Peninsula region. *Resource Geology* 50, 203-212.
- 461 Ishihara, S., Kajiwara, Y., Jin, M.S., 2002. Possible carbonate origin of ore sulfur from
462 Geumseong Mo deposit, South Koera. *Resource Geology* 52, 279-282.

- 463 Jébrak M., Marcoux É., 2015. *Geology of Mineral Resources*. Éditions Ministère de l'Énergie
464 et des Ressources Naturelles Canada, 662 p.
- 465 Klemm, L.M., Pettke, T., Heinrich, C.A., 2008. Fluid and source magma evolution of the
466 Questa porphyry Mo deposit, New Mexico, USA. *Mineralium Deposita* 43, 533-252.
- 467 Lagarde, J.L., 1987. *Granites tardi-carbonifères et déformation crustale. L'exemple de la*
468 *Meseta marocaine. Mémoires et Documents du CAES, Rennes, vol. 26 (1989) 342 p.*
- 469 Liu, J., Mao, J.W., Wu, G., Wang, F., Luo, D.F., Hu, Y.Q., Li, T.G., 2014. Fluid inclusions and H-
470 O-S-Pb isotope systematics of the Chalukou giant porphyry Mo deposit, Heilongjiang
471 Province, China. *Ore Geology Reviews*, 59, 83-96
- 472 Malinovsky, D., Hammarlund, D., Ilyashuk, B., Martinsson, O., Gelting, J., 2007. Variations in
473 the isotopic composition of molybdenum in freshwater lake systems. *Chemical*
474 *Geology* 236, 181-198, DOI: 10.1016/j.chemgeo.2006.09.006.
- 475 Marcoux, É., 1987. *Isotopes du plomb et paragenèses métalliques, traceurs de l'histoire des*
476 *gîtes minéraux. Illustration des concepts de source, d'héritage et de régionalisme*
477 *dans les gîtes français. Applications en recherche minière. Documents du BRGM,*
478 *N°117, 388p.*
- 479 Marcoux, É., Belkabir, A., Gibson, H., Lentz, D., 2008. Draa Sfar: a Hercynian pyrrhotite–Zn–
480 Cu–Pb ore deposit in the Jebilet, Morocco. *Mineralogy, geochemistry and*
481 *deformation as constrains for a genetic model features. Ore Geology Reviews* 33,
482 307–328
- 483

- 484 Markey, R., Stein, H., Morgan, J., 1998. Highly precise Re–Os dating for molybdenite using
485 alkaline fusion and NTIMS. *Talanta* 45, 935-946.
- 486 Markey, R., Stein, H.J., Hannah, J.L., Zimmerman, A., Selby, D., Creaser, R.A., 2007.
487 Standardizing Re–Os geochronology: A new molybdenite reference material
488 (Henderson, USA) and the stoichiometry of Os salts. *Chemical Geology* 244, 74-87,
489 DOI: 10.1016/j.chemgeo.2007.06.002.
- 490 Mathur, R., Brantley, S., Anbar, A., Munizaga, F., Makshev, V., Newberry, R., Vervoort, J.,
491 Hart, G., 2010. Variation of Mo isotopes from molybdenite in high-temperature
492 hydrothermal ore deposits. *Mineralium Deposita* 45, 43-50, DOI: 10.1007/s00126-
493 009-0257-z.
- 494 Moret, L., 1931. Recherches géologiques dans l'Atlas de Marrakech. Notes et Mémoires.
495 Service des Mines et Carte Géologique du Maroc, 18.
- 496 Morgan, J.W., Lovering, J.F., Ford, R.J., 1968. Rhenium and non-radiogenic osmium in
497 Australian molybdenites and other sulphide minerals by neutron activation analysis.
498 *Geological Society of Australia* 15, 189-194.
- 499 Mrini, Z., 1985. Age et origine des granitoïdes hercyniens du Maroc; Apport de la
500 géochronologie et de la géochimie isotopique (Sr, Nd, Pb). Thèse Université
501 Clermont-Ferrand, 156p.
- 502 Mrini, Z., Rafi, A., Duthou, J.L., Vidal, P., 1992. Chronologie Rb-Sr des granitoïdes hercyniens
503 du Maroc : conséquences. *Bulletin de la Société Géologique de France* 163, 281-291.
- 504 Neltner, L., 1938. Granites du Haut-Atlas. C.R. sommaire Société Géologique de France, 70-
505 71.

- 506 Ohmoto, H., 1972. Systematics of sulfur and carbon isotopes in hydrothermal ore deposits.
507 Economic Geology 67, 551–578.
- 508 Permingeat, F., 1957. Le gisement de molybdène, tungstène et cuivre d’Azegour (Haut Atlas)
509 : Etude pétrographique et métallogénique. Notes et Mémoires SGM 141, PhD thesis,
510 284p.
- 511 Poitrenaud, T., Poujol, M., Augier R., Marcoux É. – *in press*- The multi-stage story of a late-
512 Variscan W/Au deposit (Salau, French Pyrenees): Insights from REE and U/Pb LA-ICP-
513 MS analyses. Mineralium Deposita
- 514 Pomiès, C., Cocherie, A., Guerrot, C., Marcoux, É., Lancelot, J.R., 1998. Assessment of the
515 precision and accuracy of lead-isotope ratios measured by TIMS for geochemical
516 applications: example of massive sulphide deposits (Rio Tinto, Spain). Chemical
517 Geology, 144: 137-149.
- 518 Rose, A.W., Herrick, D.C., Deines, P., 1985. An Oxygen and Sulfur Isotope Study of Skarn-Type
519 Magnetite Deposits of the Cornwall Type, Southeastern Pennsylvania. Economic
520 Geology 80, 418-443.
- 521 Selby, D., Creaser, R.A., 2001a. Re-Os geochronology and systematics in molybdenite from
522 the Endako porphyry molybdenum deposit, British Columbia, Canada. Economic
523 Geology 96, 197-204.
- 524 Selby, D., Creaser, R.A., 2001b. Late and Mid Cretaceous mineralization in the Northern
525 Cordillera: Constraints from Re-Os molybdenite dates. Economic Geology 96, 1461-
526 1467.

- 527 Selby, D., Creaser, R.A., Stein, H.J., Markey, R.J., Hannah, J.L., 2007. Assessment of the ¹⁸⁷Re
528 decay constant by cross calibration of Re–Os molybdenite and U–Pb zircon
529 chronometers in magmatic ore systems. *Geochimica et Cosmochimica Acta* 71, 1999-
530 2013.
- 531 Shafiei, B., Shamanian, G., Mathur, R., Mirnejad, H., 2015. Mo isotope fractionation during
532 hydrothermal evolution of porphyry Cu systems. *Mineralium Deposita* 50, 281-291,
533 DOI: 10.1007/s00126-014-0537-0.
- 534 Shirey, S.B., Walker, R.J., 1995. Carius tube digestion for low- blank rhenium-osmium
535 analysis. *Analytical Chemistry* 67, 2136-2141.
- 536 Sillitoe, R., 2010. Porphyry copper systems. *Economic Geology*, 105, 3-41.
- 537 Smoliar, M.I., Walker, R.J., Morgan, J.W., 1996. Re-Os ages of group IIA, IIIA, IVA, and IVB
538 iron meteorites. *Science* 271, 1099-1102.
- 539 Stacey, J.S., Kramers, J.D., 1975. Approximation of Terrestrial Lead Isotope Evolution by a 2-
540 Stage Model. *Earth and Planetary Science Letters* 26, 207-221.
- 541 Timon-Sanchez, S.M., Moro Benito, M.C., Cembranos Perez, M.L., 2009. Mineralogical and
542 physiochemical evolution of the Los Santos scheelite skarn, Salamanca, NW Spain.
543 *Economic Geology*, 104, 961-995
- 544 Wen, H., Carignan, J., Cloquet, C., Zhu, X., Zhang, Y., 2010. Isotopic delta values of
545 molybdenum standard reference and prepared solutions measured by MC-ICP-MS:
546 Proposition for delta zero and secondary references. *Journal of Analytical Atomic*
547 *Spectrometry* 25, 716-721, DOI: 10.1039/B921060A.

Sample	Location	wt(g)	Re(ppm)	±	¹⁸⁷ Re(ppm)
Mo78	Tizgui mine	0.021	14.00	0.05	8.80
Mo86b	Azegour mine	0.020	7.00	0.03	4.40
Mo89b	Azegour mine	0.100	2.87	0.01	1.80

*uncertainty includes that associated with the decay constant

ID	Location	n	$\delta^{97}\text{Mo}_{\text{NIST}}$	2σ
Mo004	Azegour mine	6	0.05	0.09
Mo007	Azegour mine	6	-0.29	0.08
Mo008	Azegour mine	6	0.21	0.05
Mo072	Azegour mine	5	-0.35	0.06
Mo073	Azegour mine	6	-0.40	0.09
Mo074a	Azegour mine	5	0.21	0.07
Mo074b	Azegour mine	5	-0.08	0.03
Mo074c	Azegour mine	6	-0.02	0.05
Mo075a	Azegour mine	6	0.13	0.09
Mo075b	Azegour mine	6	0.23	0.07
Mo076a	Azegour mine	6	-0.08	0.07
Mo076b	Azegour mine	6	0.32	0.07
Mo077	Tizgui mine	6	0.30	0.07
Mo078	Tizgui mine	6	0.08	0.10
Mo084a	Azegour mine	5	-0.18	0.04
Mo084b	Azegour mine	5	-0.09	0.02
Mo084c	Azegour mine	5	-0.20	0.02
Mo085a	Azegour mine	5	-0.09	0.09
Mo085b	Azegour mine	5	0.02	0.08
Mo085c	Azegour mine	5	-0.14	0.04
Mo085d	Azegour mine	5	-0.08	0.03
Mo086a	Azegour mine	8	-0.13	0.09
Mo086b	Azegour mine	5	-0.18	0.07
Mo087	Azegour mine	5	0.18	0.06
Mo088a	Azegour mine	5	0.03	0.05
Mo088b	Azegour mine	5	0.17	0.07
Mo089a	Azegour mine	5	0.03	0.07
Mo089b	Azegour mine	5	0.27	0.04
Mo090	Azegour mine	5	0.11	0.04

ID	Location	Mineral
AZM 3c	Azegour mine	Chalcopyrite
AZM 3d	Azegour mine	Chalcopyrite
AZM 4a	Azegour mine	Chalcopyrite
AZM 4b	Azegour mine	Chalcopyrite
AZM5	Azegour mine	Chalcopyrite
AZM 3a	Azegour mine	Pyrrhotite
AZM 3b	Azegour mine	Pyrrhotite
AZT 1a	Tizgui road	Pyrrhotite
AZT 1b	Tizgui road	Pyrrhotite
Mo 4	Azegour mine	Molybdenite
Mo 7	Azegour mine	Molybdenite
Mo 8	Azegour mine	Molybdenite
Mo 72	Azegour mine	Molybdenite
Mo 73	Azegour mine	Molybdenite
Mo 74a	Azegour mine	Molybdenite
Mo 74b	Azegour mine	Molybdenite
Mo 74c	Azegour mine	Molybdenite
Mo 75a	Azegour mine	Molybdenite
Mo 75b	Azegour mine	Molybdenite
Mo 76a	Azegour mine	Molybdenite
Mo 76b	Azegour mine	Molybdenite
Mo 77	Tizgui mine	Molybdenite
Mo 78	Tizgui mine	Molybdenite
Mo 84a	Azegour mine	Molybdenite
Mo 84b	Azegour mine	Molybdenite
Mo 84c	Azegour mine	Molybdenite
Mo 85a	Azegour mine	Molybdenite
Mo 85b	Azegour mine	Molybdenite
Mo 85c	Azegour mine	Molybdenite
Mo 85d	Azegour mine	Molybdenite
Mo 86a	Azegour mine	Molybdenite
Mo 86b	Azegour mine	Molybdenite
Mo 87	Azegour mine	Molybdenite
Mo 88a	Azegour mine	Molybdenite
Mo 88b	Azegour mine	Molybdenite

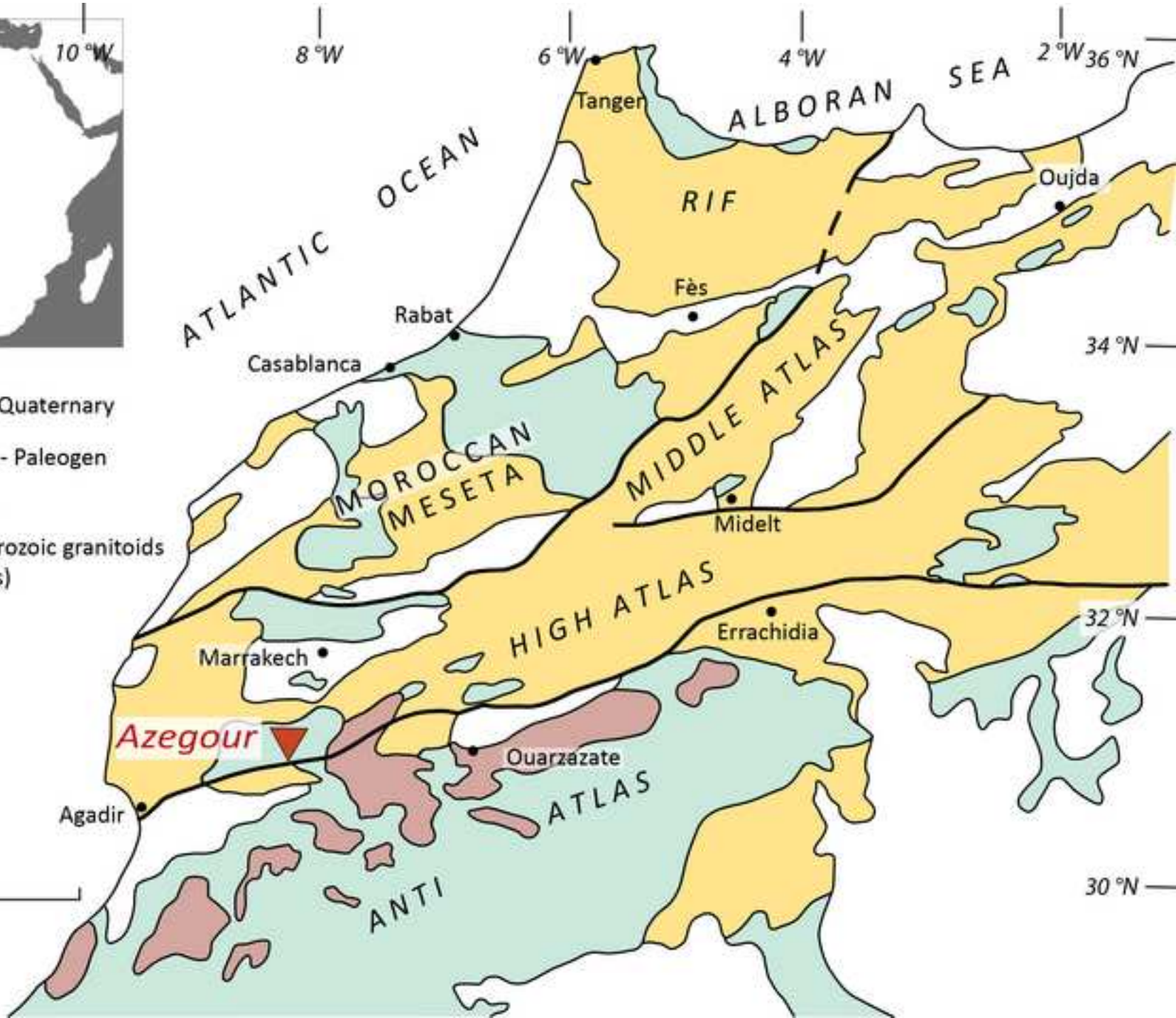
Description			Content	
Mineral	Name	Provenance	U ppm	Th ppm
Pyrrhotite	AZT1a	Tizgui Road	0.60	0.14
	AZT1b	Tizgui Road	0.24	0.13
	AZM3a	Azegour Mine	2.57	0.09
	AZM3b	Azegour Mine	0.04	0.04
Chalcopyrite	AZM3c	Azegour Mine	0.44	0.10
	AZM3d	Azegour Mine	0.40	0.06
	AZM4a	Azegour Mine	0.05	0.03
	AZM4b	Azegour Mine	0.10	0.02
	AZM5	Azegour Mine	0.04	0.02
Molybdenite	Mo4	Azegour Mine	0.22	0.05
	Mo7	Azegour Mine	1.05	0.04
	Mo8	Azegour Mine	1.13	0.04
K-Feldspar	AZG	Azegour granite	0.81	0.53

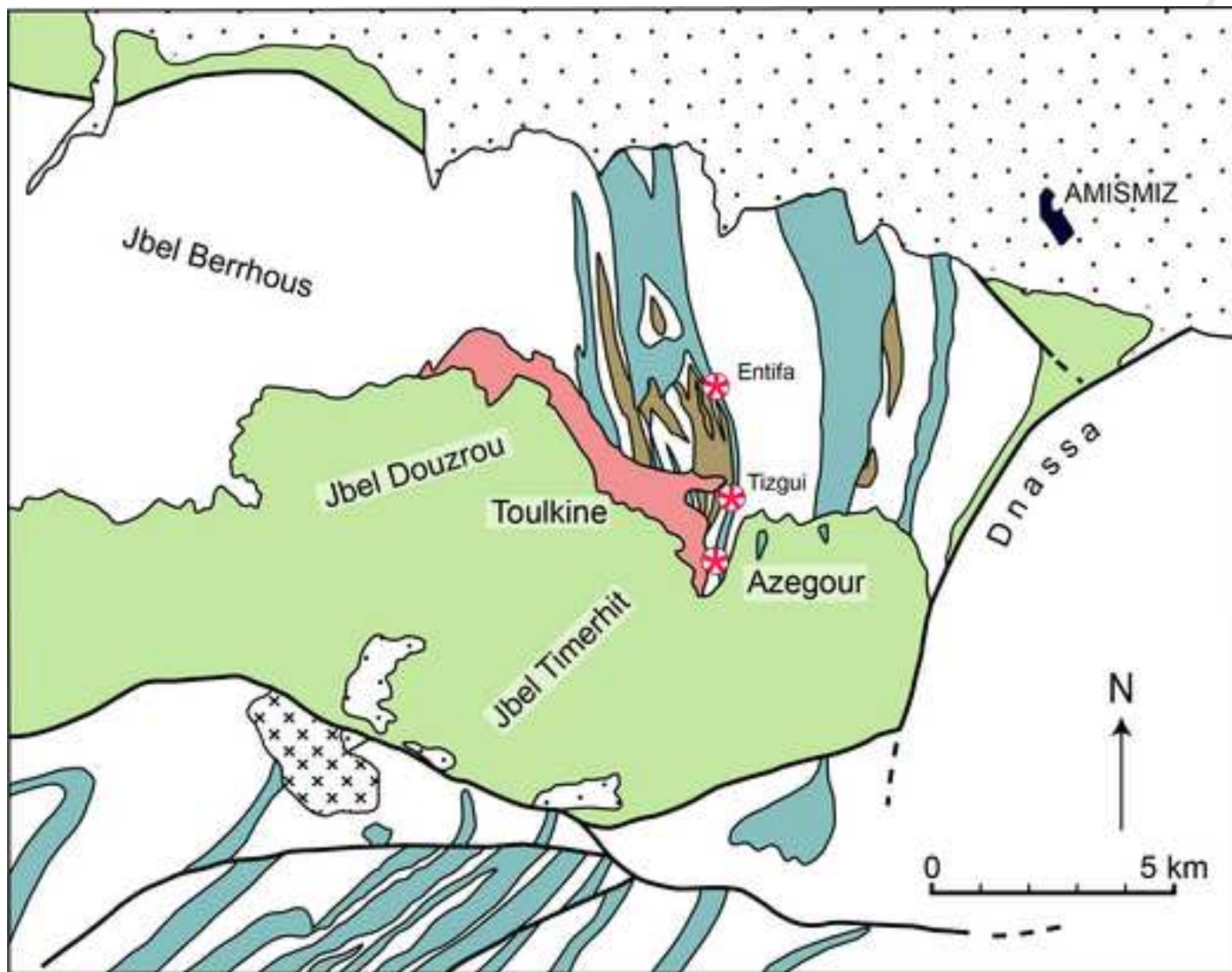


- Neogen - Quaternary
- Mesozoic - Paleogen
- Paleozoic
- Neoproterozoic granitoids (Anti Atlas)





200 km


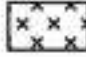








Post-Paleozoic

-  Tertiary and Quaternary formations
-  Cretaceous and Jurassic limestones

Late Paleozoic

-  Azegour granite
-  quartz-diorite

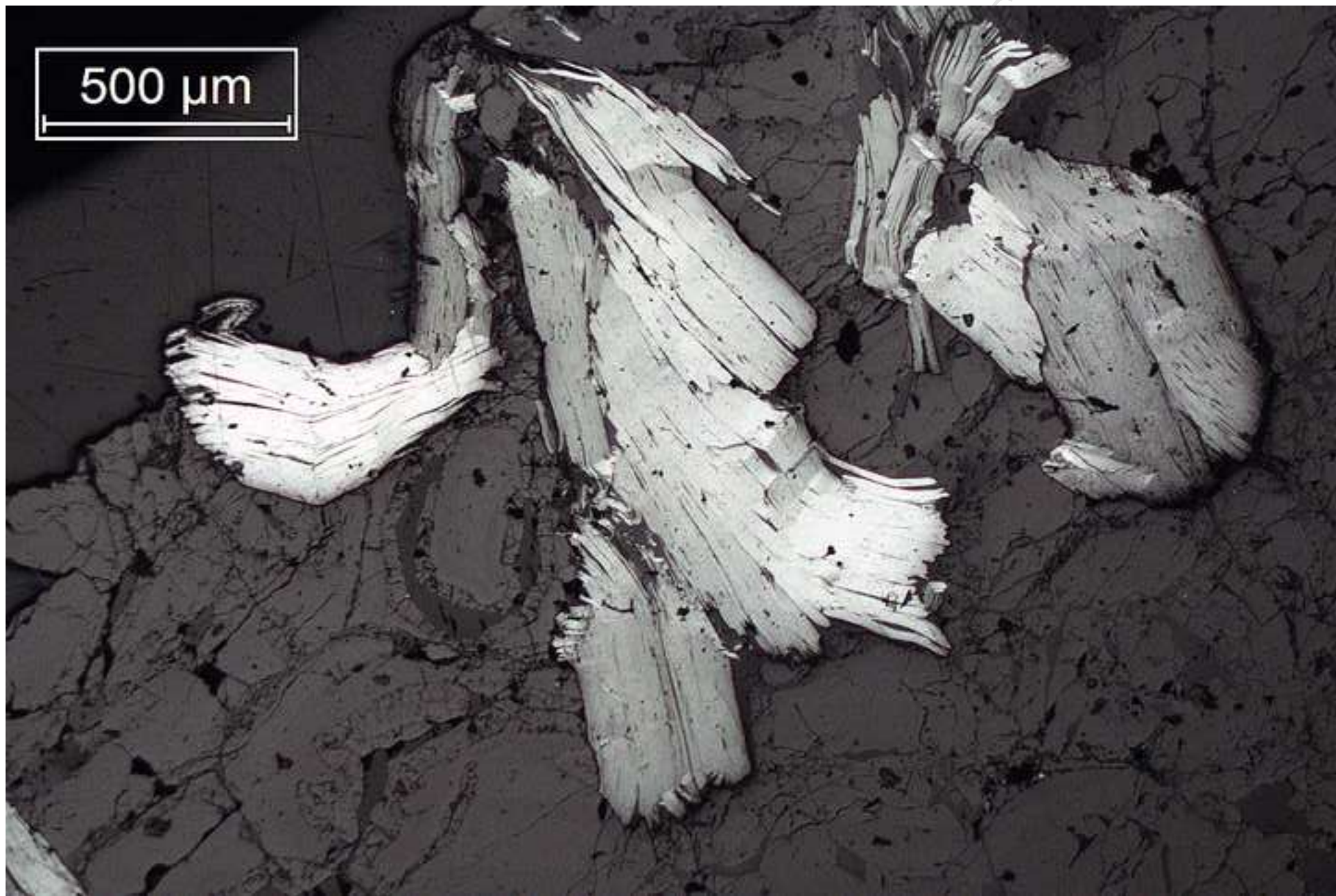
Cambrian

-  limestone and dolostone
-  volcanic unit
-  shales and sandstones
-  molybdenum mines



granite

skarn



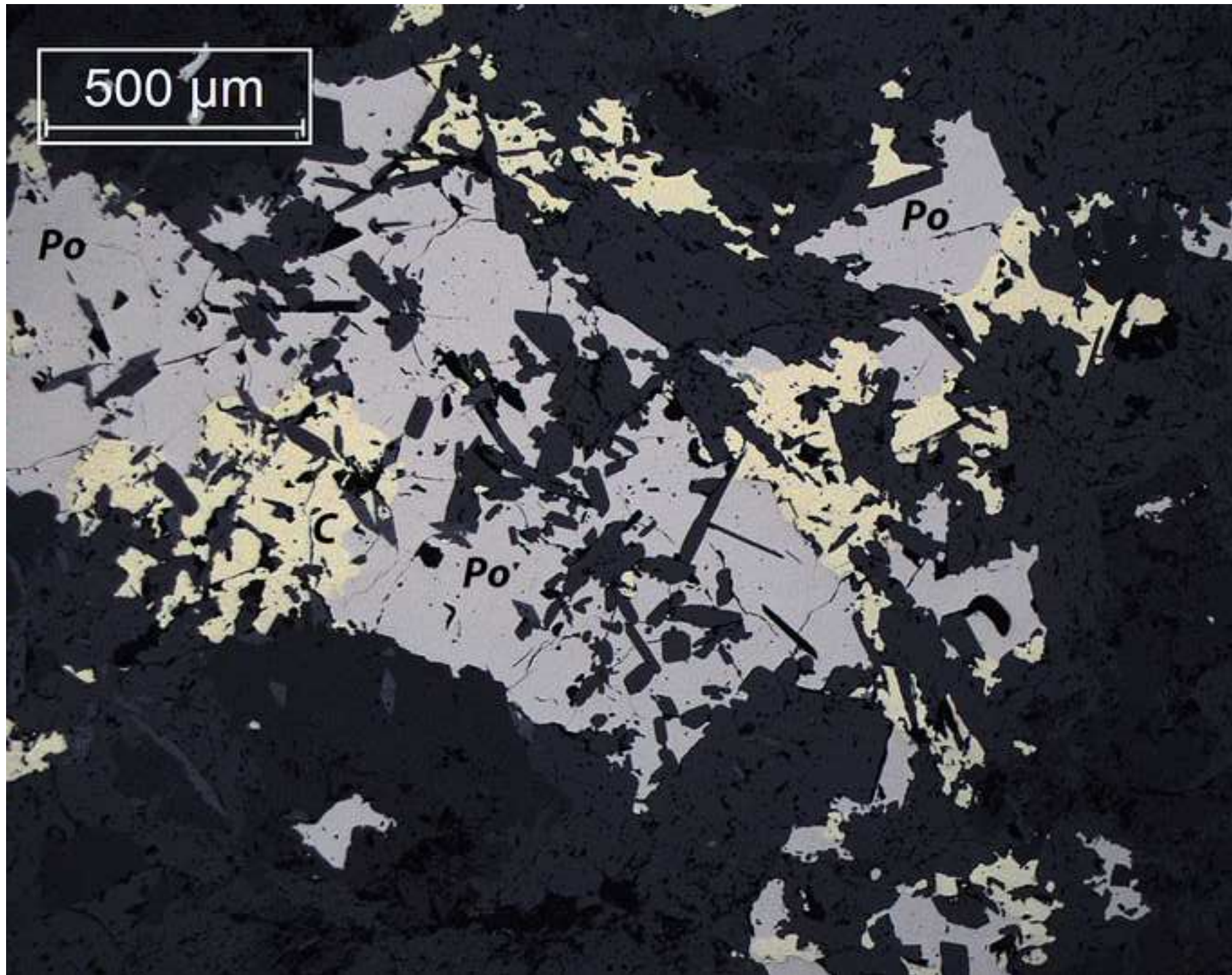
500 μm

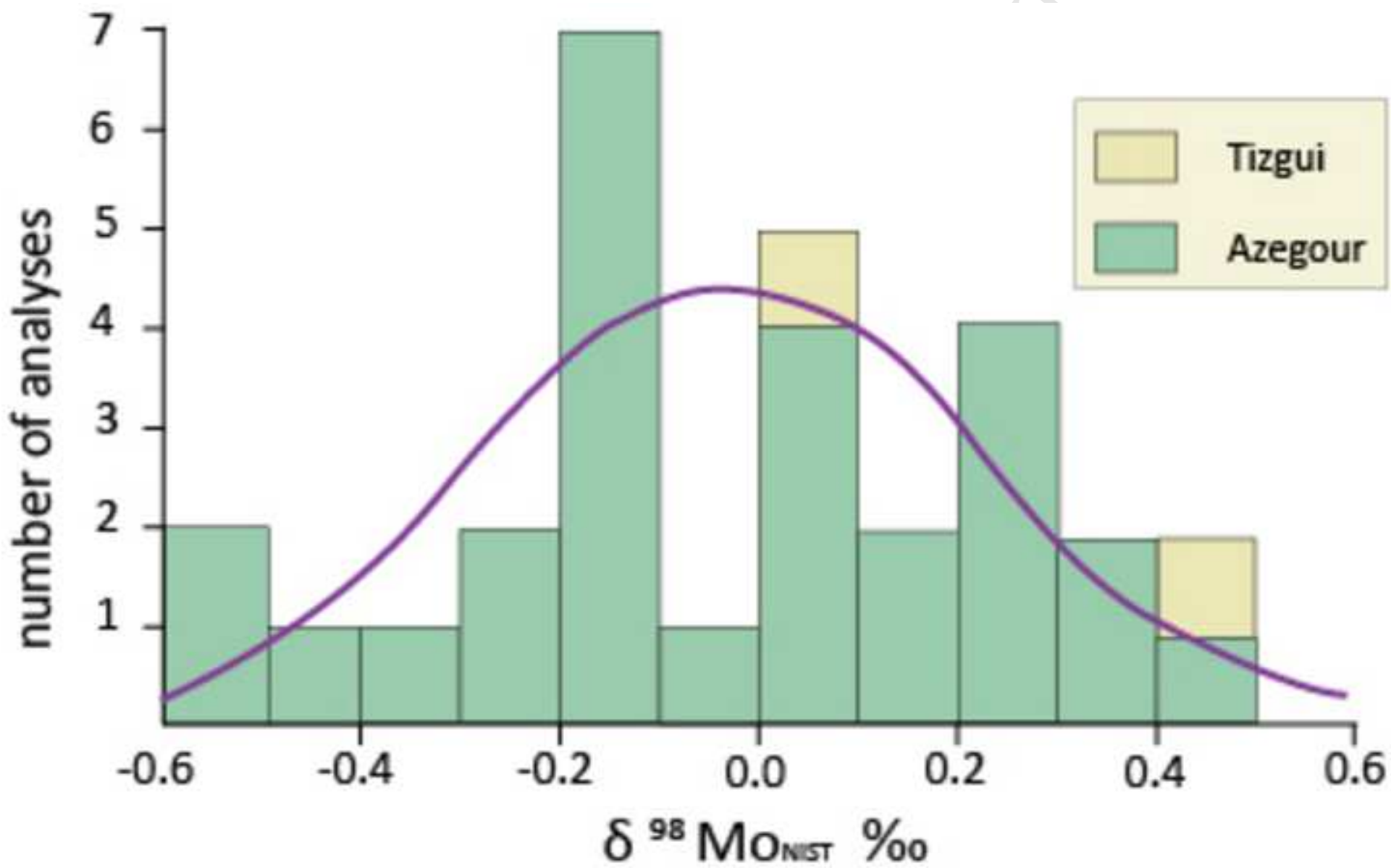
Po

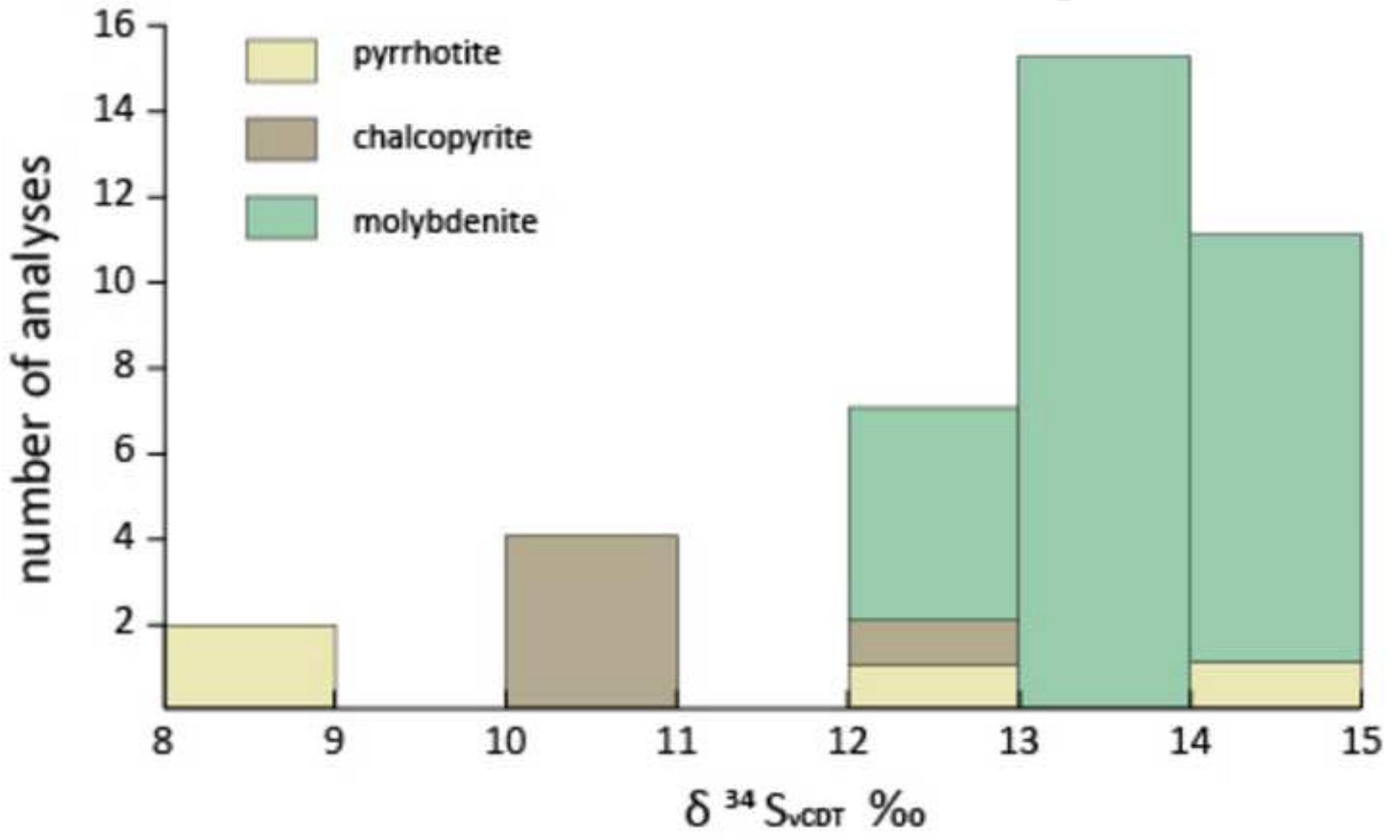
Po

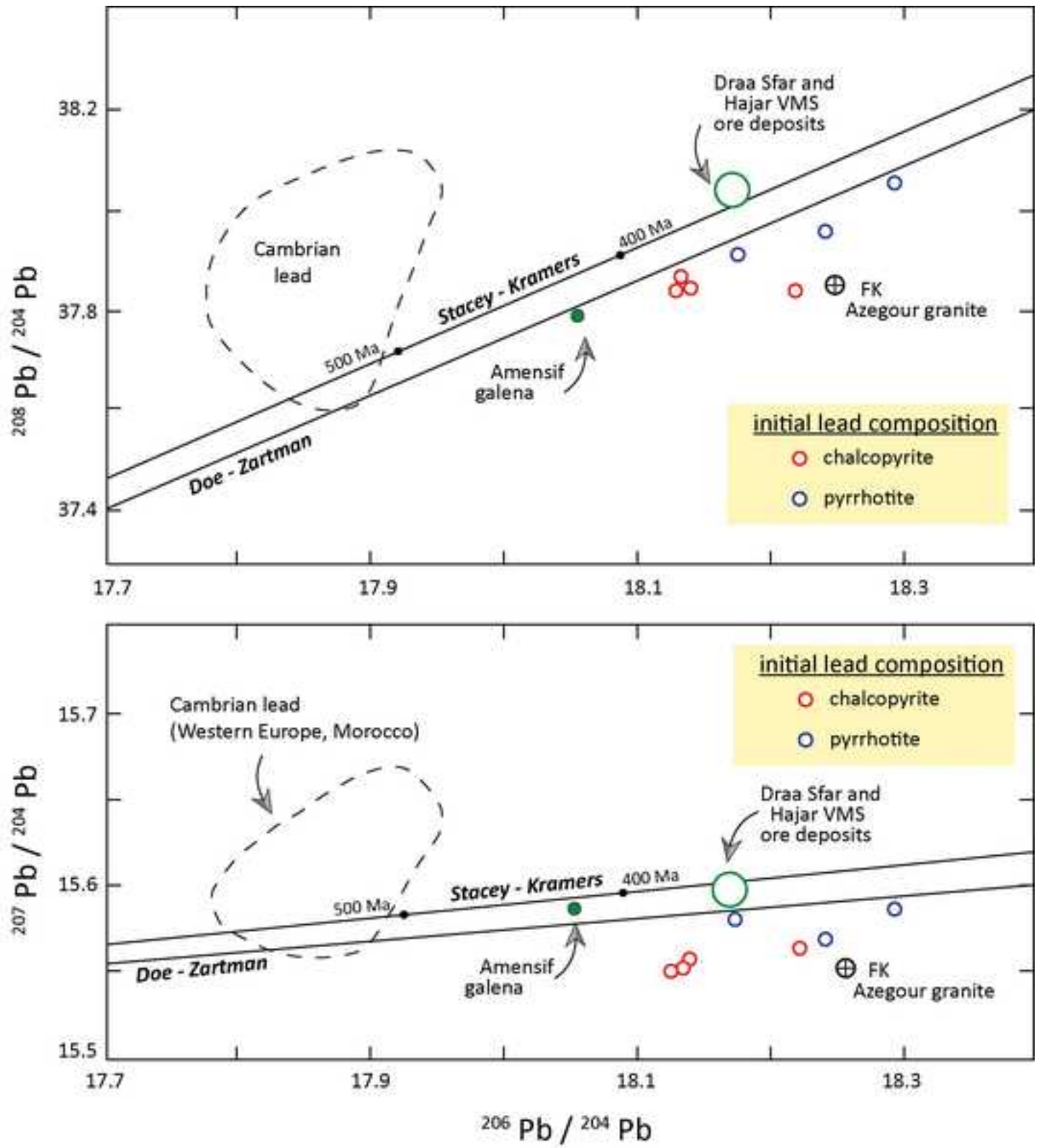
C

Po









Highlights

- The Mo-Cu-W Azegour skarn is Permian (276 ± 1.2 Ma, Re-Os geochronology)
- Multiple Permian mineralization events associated with the Azegour granite are likely
- $\delta^{34}\text{S}$ values determined from sulphides suggest a sedimentary origin for sulphur
- Source of common lead has to be sought in the host Cambrian volcano-sedimentary units